J Nanostruct Chem (2017) 7:121–132
DOI 10.1007/s40097-017-0226-5

ORIGINAL RESEARCH

A novel nitrogen dioxide gas sensor based on TiO_2-supported Au nanoparticles: a van der Waals corrected DFT study

Amirali Abbasi[1,2,3] · **Jaber Jahanbin Sardroodi**[1,2,3]

Received: 18 February 2017 / Accepted: 6 May 2017 / Published online: 15 May 2017

Abstract The interactions of nitrogen dioxide molecule with TiO_2-supported Au nanoparticles were investigated using density functional theory. Surface Au atoms on the TiO_2-supported Au overlayer were found to be the most favorable binding sites, thus making the adsorption process very strong. Both oxygen and nitrogen atoms of the NO_2 molecule can bind to the Au surface by forming strong chemical bonds. The adsorption of NO_2 molecule on the considered structures gives rise to significant changes in the bond lengths, bond angles, and adsorption energies of the complex systems. The results indicate that NO_2 adsorption on the TiO_2-supported Au nanoparticle by its oxygen atoms is energetically more favorable than the NO_2 adsorption by its nitrogen atom, indicating the strong binding of NO_2 to the TiO_2-supported Au through its oxygen atoms. Thus, the bridge configuration of TiO_2/Au + NO_2 is found to be the most stable configuration. Both oxygen and nitrogen atoms of NO_2 move favorably towards the Au surface, as confirmed by significant overlaps in the PDOSs of the atoms that forming chemical bonds. This study not only suggests a theoretical basis for gas-sensing properties of the TiO_2-supported Au nanoparticles, but also offers a rational approach to develop nanostructure-based chemical sensors with improved performance.

Keywords Density functional theory · NO_2 · TiO_2-supported Au nanoparticle · PDOS

Introduction

TiO_2 is one of the most broadly studied transition metal semiconductors with outstanding properties, such as non-toxicity, high catalytic efficiency, and extensive bandgap [1]. Until now, various kinds of well-known applications have been proposed for TiO_2, such as photo-catalysis, gas sensor devices, organic dye-sensitized solar cells, water splitting, and air pollution control [2–5]. Anatase, rutile, and brookite are the most important polymorphs of TiO_2 [6]. Of the three polymorphs of TiO_2, the rutile form is found to be the most stable phase. There is not any detailed theoretical investigation on the physical and chemical properties of brookite because of its metastable property. This meta-stability results in some troubles during the synthesis of brookite [7]. The improved reactivity of anatase is comparable with that of rutile and brookite phases [8–14]. Anatase has been extensively studied due to its enhanced activity in some photo-catalysis reactions, such as TiO_2-supported metal particle reactions, compared to the rutile and brookite phases [15–17]. Unfortunately, as a most promising material, the widely application of TiO_2-based gas sensors is influenced by its wide bandgap (3–3.2 eV). This results in the absorption of a small percentage of the incoming solar light (3–5%). An enormous amount of effort has been invested in enhancing the optical response of TiO_2 by nitrogen doping [8].

Electronic supplementary material The online version of this article (doi:10.1007/s40097-017-0226-5) contains supplementary material, which is available to authorized users.

✉ Amirali Abbasi
a_abbasi@azaruniv.edu

[1] Molecular Simulation Laboratory (MSL), Azarbaijan Shahid Madani University, Tabriz, Iran

[2] Department of Chemistry, Faculty of Basic Sciences, Azarbaijan Shahid Madani University, Tabriz, Iran

[3] Computational Nanomaterials Research Group (CNRG), Azarbaijan Shahid Madani University, Tabriz, Iran

Recently, gold was considered as an inactive metal, which possesses less activity than the other metals in many reactions. Haruta and co-workers showed that gold particles can increase the combustion of CO molecule and promote different catalytic reactions [18]. The gold particles supported by metal oxides (oxide-supported gold particles) have gained more attention due to their higher activities in the surface processes [19–22]. This leads to the structures with enhanced catalytic activity and higher stability [23, 24]. There are a large number of important reactions, in which the oxide-supported Au overlayers play a key role, including the epoxidation of C_3H_6 [25], reduction of NO_x molecules [26], and dissociation of SO_2 molecule [27]. TiO_2 has been considered as one of the most appropriate support materials for gold particles [28, 29]. The interactions of gold nanoparticles with TiO_2 (rutile and anatase) have been widely studied in the last few years. Vittadini et al. considered the adsorption behaviors of gold clusters on the TiO_2 anatase (101) surfaces [30]. Metiu and co-workers investigated the adsorption site and electronic structures of the TiO_2 rutile-supported Au nanoparticles [31].

The adsorption of the O_2 and CO_2 on gold nanoparticles supported by TiO_2 has been investigated by DFT calculations [32]. The main source of nitrogen dioxide emission is internal combustion engines, burning fossil fuels. It also results from cigarette smoke, kerosene heaters, and vehicle engines and stoves. Thus, finding an efficient sensor for the removal of this toxic molecule is an important issue to public health and environmental protection [33]. An ideal semiconductor oxide-based gas sensor should have properties, such as high sensitivity to the expected toxic material, low price fabrication, and compatibility with modern electronic devises. Among different gas sensors, the oxide-supported gold nanoparticles have been characterized as efficient sensor materials because of their higher activities. Therefore, establishing multi-component structures in sensor materials has long been regarded as the best strategy for improving the sensing performance of TiO_2 particles. The mechanism of gas sensing for the removal of toxic NO_2 molecules by metal oxide-based sensors is represented in Fig. 1. We have decided to perform a DFT study of the interaction of NO_2 molecule with the TiO_2-supported Au overlayers to fully exploit the gas-sensing capabilities of these nanocomposites.

The consecutive adsorption of NO_2 molecules on the TiO_2-supported Au overlayers probably produces N_2 molecule formed from the central nitrogen atoms of the two adsorbed NO_2 molecules. This is a consequence of the formation of weak chemical bonds between oxygen atoms of NO_2 molecule and Ti sites of the adsorbent. This leads to weakening of the bond between central nitrogen and the side oxygen atoms of the adsorbed NO_2 molecules. Based

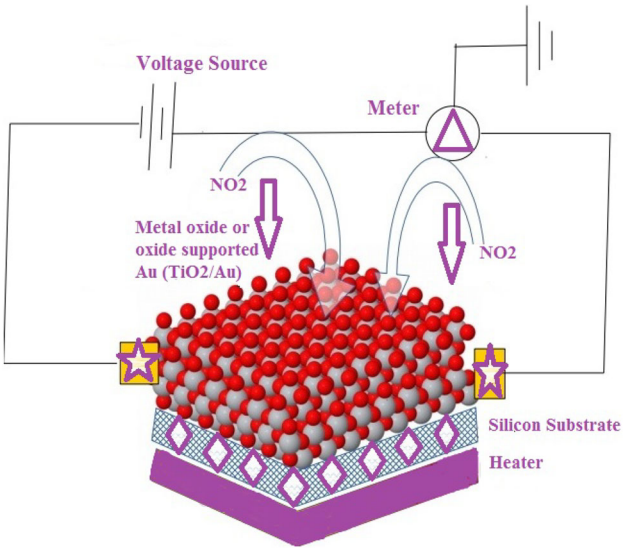

Fig. 1 Schematic drawing of a typical metal oxide-based gas sensor

on this fact, we can conclude desorption of NO_2 molecule from the surface of the TiO_2-supported Au overlayer. The next NO_2 molecule then can be adsorbed on the considered nanocomposite, and this consecutive process was repeated over and over again to obtain the enhanced sensing performance of the adsorbent material. Figure 1 shows a schematic structure of a metal oxide-based gas sensor. We have also commented on the charge analysis of the complex system according to the Mulliken population analysis. In this study, the main objective is to perform a systematic investigation on the adsorption behaviors of the TiO_2-supported Au nanoparticles as potentially efficient gas sensors for NO_2 detection.

Computational methods

Details of computation

All of DFT calculations [34, 35] were carried out using the Open source Package for Material eXplorer (OPENMX3.8) [36]. OPENMX is an efficient software package for nanoscale materials simulations based on norm-conserving pseudo-potentials and pseudo-atomic localized basis functions [37, 38]. To optimize the structures, the pseudoatomic orbitals (PAOs) centered on atomic sites were used as basis sets. The calculations were done with a considered energy cutoff of 150 Ry. Pseudo-atomic orbitals were constructed by minimal basis sets (three *s*-state, three *p*-state, and one *d*-state radial functions) for the Ti, (three *s*-state, three *p*-state, two *d*-state, and one *f*-state radial functions) for the Au, and (two *s*-state, two *p*-state radial functions) for O and N atoms, within cut-off radii of basis functions set to the

values of seven for Ti, nine for Au, and five for O and N (all in Bohrs). The total energy of the system was computed within the Perdew–Burke–Ernzerhof (PBE) form of the generalized gradient approximation (GGA) exchange–correlation potential [39]. Mulliken population analysis was also conducted to fully analyze the charge transfer between NO_2 and nanocomposite. To optimize the adsorption configurations of the TiO_2-supported Au overlayers with adsorbed NO_2 molecules, all atoms of the system are entirely relaxed until the force on each atom is less than 0.01 eV/Å. The size of the simulation box containing pristine TiO_2-supported Au nanoparticles is 20 Å × 20 Å × 30 Å, being larger than the realistic size of the composite system.

Three possible orientations of NO_2 towards the TiO_2-supported Au nanoparticles are studied in this work. XCrysDen program was used for visualization of the figures presented in this study [40]. The total number of atoms of the nanocomposite in the considered box is 88 atoms (16 Au, 48 O, and 24 Ti atoms) of undoped TiO_2-supported Au overlayer. The effects of vdW interactions were also taken into account in this study. Both LDA and GGA methods cannot describe the vdW interactions in the systems, such as NO_2 adsorption, on the TiO_2-supported Au nanoparticles. Thus, an inclusion of additional functional into standard DFT methods would be required, which correctly describes the effects of vdW interactions. Grimme's DFT-D2 [41] and DFT-D3 methods [42, 43] were used in this study to correct the adsorption energies for dispersion energy. The adsorption energy, E_{ad}, is estimated as the following equation:

$$E_{ad} = E_{(composite+adsorbate)} - E_{composite} - E_{adsorbate} \quad (1)$$

where $E_{(composite\ +\ adsorbate)}$ is the total energy of the TiO_2-supported Au overlayers with adsorbed NO_2, $E_{composite}$ is the energy of bare TiO_2-supported Au overlayer, and $E_{adsorbate}$ represents the energy of a free gas-phase NO_2 molecule. As distinct from this equation, the adsorption energies of energy favorable configurations are negative.

Modeling TiO_2-supported Au nanoparticles

We have constructed TiO_2 anatase nanoparticle using a 3 × 2 × 1 supercell of TiO_2 anatase. The considered unit cell is available at "American Mineralogists Database" webpage [44] and reported by Wyckoff [45]. The size of the studied nanoparticles was chosen following Lei et al. [46] and Liu et al. [47]. The results published by Lei et al. [46] show that the smaller the particle is, the higher the

Table 1 Calculated surface energies (in J/m^2) for the anatase (0 0 1) and (1 0 1) surfaces, calculated based on GGA pseudo-potential

Surface	(0 0 1)	(1 0 1)
Calculated	0.96	0.49
Literature	0.98	0.49

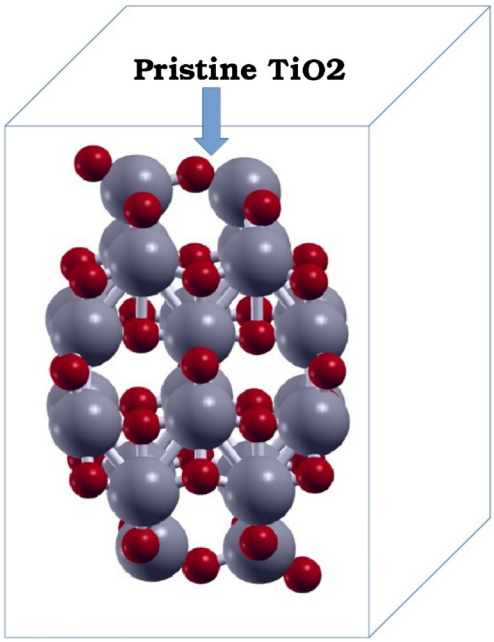

Fig. 2 Representation of a pristine TiO_2 anatase nanoparticle, two dangling oxygen atoms were used to set a 1:2 atomic charge ratio between the oxygen and titanium atoms

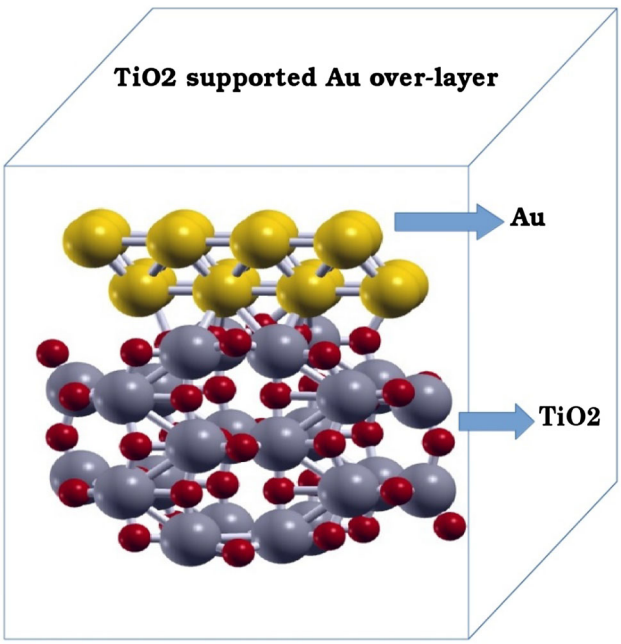

Fig. 3 Optimized geometry of undoped TiO_2-supported Au overlayer. The *yellow*, *gray,* and *red balls* denote gold, titanium, and oxygen atoms, respectively. TiO_2 was demonstrated to an appropriate support material for gold particles

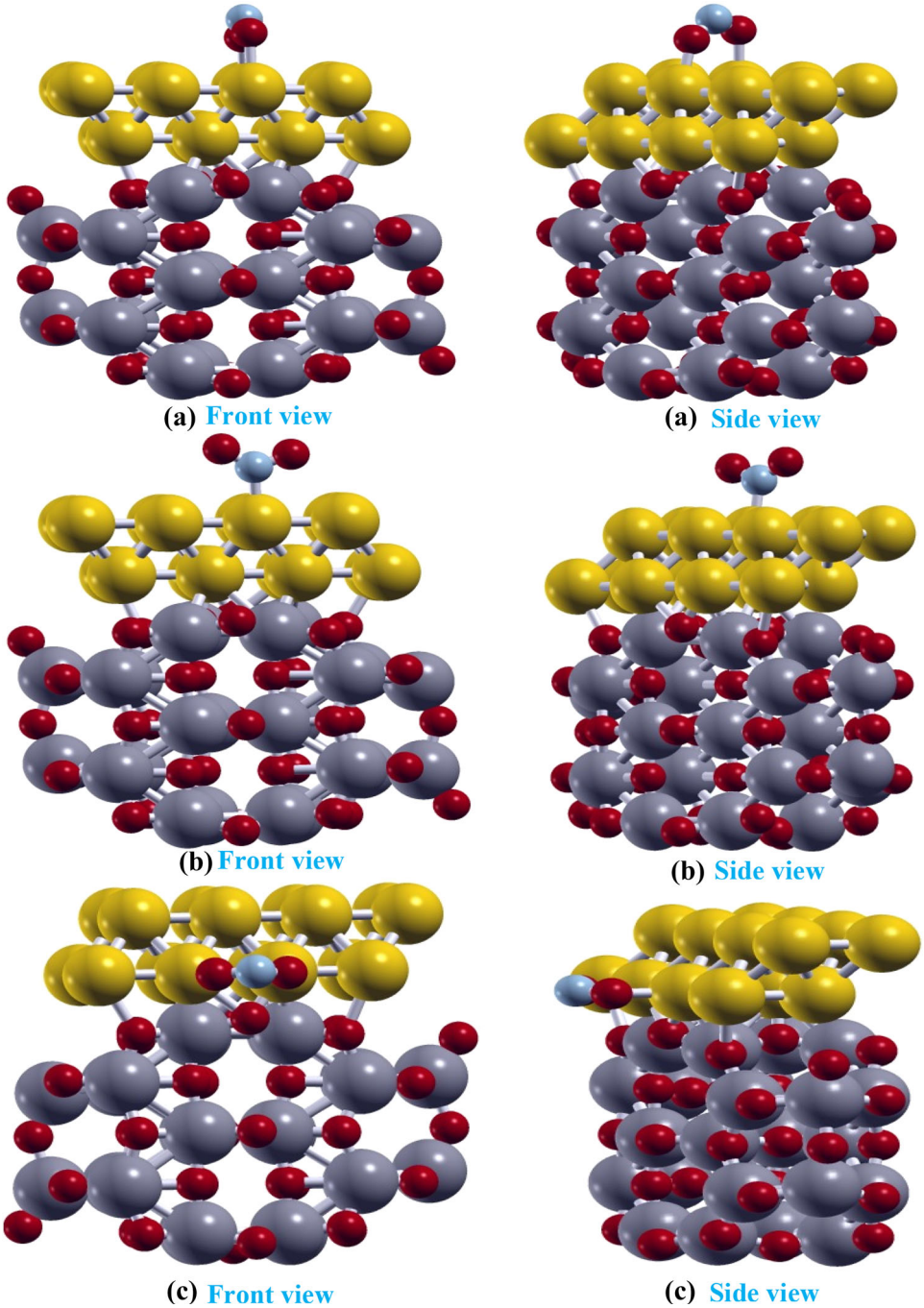

Fig. 4 Optimized geometry configurations of the NO_2 molecule adsorbed on the undoped TiO_2-supported Au overlayers in different orientations, **a** NO_2 adsorption on the *top*-Au sites by its oxygen atoms (configuration A), **b** NO_2 adsorption on the *top*-Au site by its nitrogen atom (configuration B), and **c** NO_2 adsorption on the *side*-Au sites by its oxygen atoms (configuration C)

average energy is. They have explained that the nanoparticles containing 72 atoms have the lowest energy (the highest stability among the different types of nanoparticles. The optimized structure of the pristine TiO_2 nanoparticle is shown in Fig. 2. The constructed structure of pristine TiO_2 nanoparticle was geometrically optimized and then coupled with Au nanoparticle to model a metal oxide-supported Au overlayer. The calculated structural parameters for the chosen Au nanoparticle are listed in Table S1. The atomic number ratio between titanium and oxygen atoms should

Table 2 Bond lengths (in Å) and angles (in degrees) of NO_2 molecule adsorbed on the TiO_2-supported Au nanoparticles

Complex type	Au–O_1	Au–O_2	Au–N	N–O_1	N–O_2	O–N–O
Undoped						
A	2.23	2.36	–	1.32	1.34	120.4
B	–	–	2.19	1.30	1.31	122.8
C	2.34	2.36	–	1.32	1.32	120.7
Non-adsorbed	–	–	–	1.20	1.20	134.3

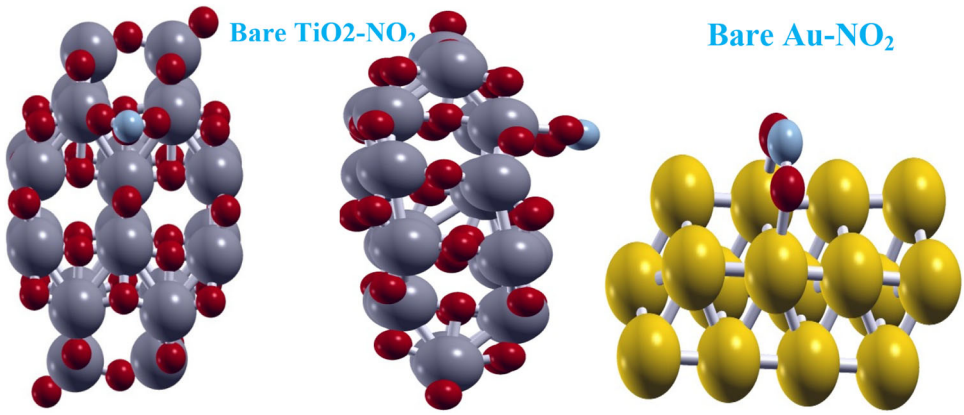

Fig. 5 Optimized geometry configurations of the NO_2 molecule adsorbed on the bare TiO_2 and Au nanoparticles

Table 3 Adsorption energies (in eV) and Mulliken charge values (in *e*) for NO_2 molecule adsorbed on bare TiO_2, bare Au, and TiO_2-supported Au overlayers

Type of complex	Adsorption energy (eV)			Mulliken charge (normal basis sets)	Mulliken charge (large basis sets)
	PBE	DFT-D2	DFT-D3		
Undoped					
A	−2.18	−4.12	−8.04	0.15	0.37
B	−1.41	−2.70	−2.08	0.25	0.47
C	−1.87	−3.60	−7.06	0.16	0.38
Bare TiO_2	−0.72	−1.44	−2.86	+0.05	0.27
Bare Au	−1.23	−2.24	−4.06	+0.04	0.26

be set as 1:2, which was obtained by setting two dangling oxygen atoms in TiO_2. Spin polarization is not used for the optimization of pristine TiO_2 particles due to the even electron number of pure particles. During the optimization process, "Cluster" method was used as efficient eigenvalue solver. For electronic structure calculations, the convergence criterion of 1.0×10^{-6} Hartree was used, whereas the criterion for geometry optimization was set at 1.0×10^{-4} Hartree/bohr. In addition, "Opt" was used as geometry optimizer, which presents a robust scheme for optimization of solid-state structures based on cluster method.

The surface energies for TiO_2 anatase were computed and summarized in Table 1. The calculated data from GGA are in reasonable agreement with the experimentally reported data or other computational works [48]. It indicates that GGA pseudo-potential possesses a reasonable accuracy for calculating the properties of anatase particles. The energy calculations were carried out at the Γ point. The considered simulation box has the dimension of 20 Å × 15 Å × 30 Å. To reduce the additional interactions between neighbor particles, a 11.5 Å distance in three directions was considered.

TiO_2 includes two types of titanium atoms, namely, five-fold coordinated (5f-Ti) and six-fold coordinated (6f-Ti), as well as two types of oxygen atoms, indicated by three-fold coordinated (3f-O) and two-fold coordinated (2f-O) atoms [49, 50]. For the bent geometry of the NO_2 molecule, the calculated N–O bond length and O–N–O bond angle are about 1.20 Å and 134.3°, respectively, which agree reasonably with the previous gas-phase data [51]. Au nanoparticle was supported by TiO_2 anatase to model a TiO_2-supported Au overlayer. Figure 3 displays the equilibrium structure of the undoped TiO_2-supported Au nanoparticle.

Results and discussion

Structural parameters and adsorption energies

Three possible orientations of the NO_2 molecule towards the TiO_2-supported Au overlayers were considered, in which the NO_2 molecule can bind to the surface of Au atoms either by its nitrogen or by oxygen atoms. The relevant configurations of NO_2 adsorption on the TiO_2-supported Au nanoparticles are shown in Fig. 4, as indicated by adsorption types A–C. We found that the NO_2 interaction with Au atoms is stronger than the interaction with TiO_2 nanoparticle. Thus, the surfaces of Au atoms are strongly favored during the adsorption process. Over the TiO_2-supported Au nanoparticle, the NO_2 molecule

preferentially interacts with the Au nanoparticle. The interaction by oxygen atoms leads to a bridge configuration of NO_2 on the nanocomposite. As a closer comparison, it is of eminent importance to describe the adsorption configurations and relative orientations in detail. Configuration A shows the adsorption of NO_2 on the top-site Au atoms of the TiO_2-supported Au, while configuration C represents the interaction of NO_2 with the lateral-site Au atoms. In configuration B, we can see that NO_2 molecule interacts with the top-site Au atoms by its nitrogen atom, providing a single contacting point between NO_2 and nanocomposite. Configurations A and C indicate a double contacting point between NO_2 and TiO_2-supported Au. Figure S1 also displays the top views of NO_2 molecule adsorbed on the TiO_2-supported Au overlayers.

Table 2 summarizes the lengths and distances for the newly formed Au–O bonds, N–O bonds of the adsorbed NO_2 molecule, and O–N–O bond angles of NO_2 after the adsorption process. Based on the obtained results, we found that the N–O bonds of the adsorbed NO_2 molecule were elongated due to the considerable electronic density shifts from the Au–Au bonds of Au nanoparticle and N–O bonds of the NO_2 molecule to the newly formed Au–O and Au–N bonds between the nanocomposite and NO_2. Thus, the adsorption process results in weakening the N–O bonds of the NO_2 molecule. The O–N–O bond angles of NO_2 were increased compared to those of non-adsorbed NO_2 molecule. This increase in the bond angles could be mostly attributed to the elongation of the N–O bonds of the adsorbed NO_2 molecule. In configuration B, the bond angle increase and geometry changing could be ascribed to the formation of new Au–N bond. The formation of new bond is a key reason, which is responsible for changing the *sp* hybridization of the nitrogen atom in the NO_2 molecule to hybridization with higher *p* contribution (near-sp^2). Consequently, the *p* characteristics of bonding molecular orbitals of the nitrogen atom in the adsorbed NO_2 molecule become higher.

For clear comparison, the adsorption configurations of NO_2 molecule on pristine Au and TiO_2 nanoparticles are also represented in Fig. 5, indicating less stable adsorption of NO_2 on the considered bare nanoparticles. Table 3

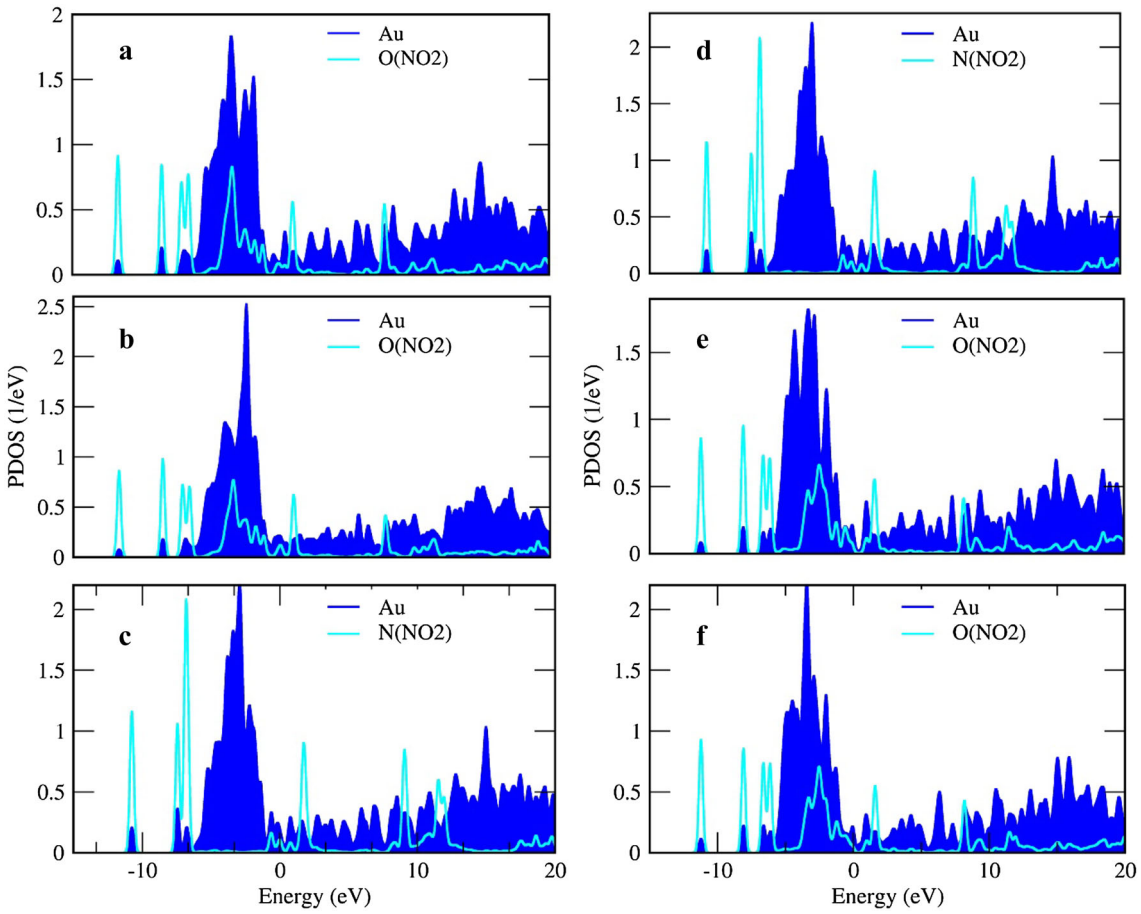

Fig. 6 PDOSs for the adsorption complexes of the undoped TiO_2-supported Au nanoparticles with adsorbed NO_2 molecules. (**a**, **b**) complex A; (**c**, **d**) complex B; (**e**, **f**) complex C

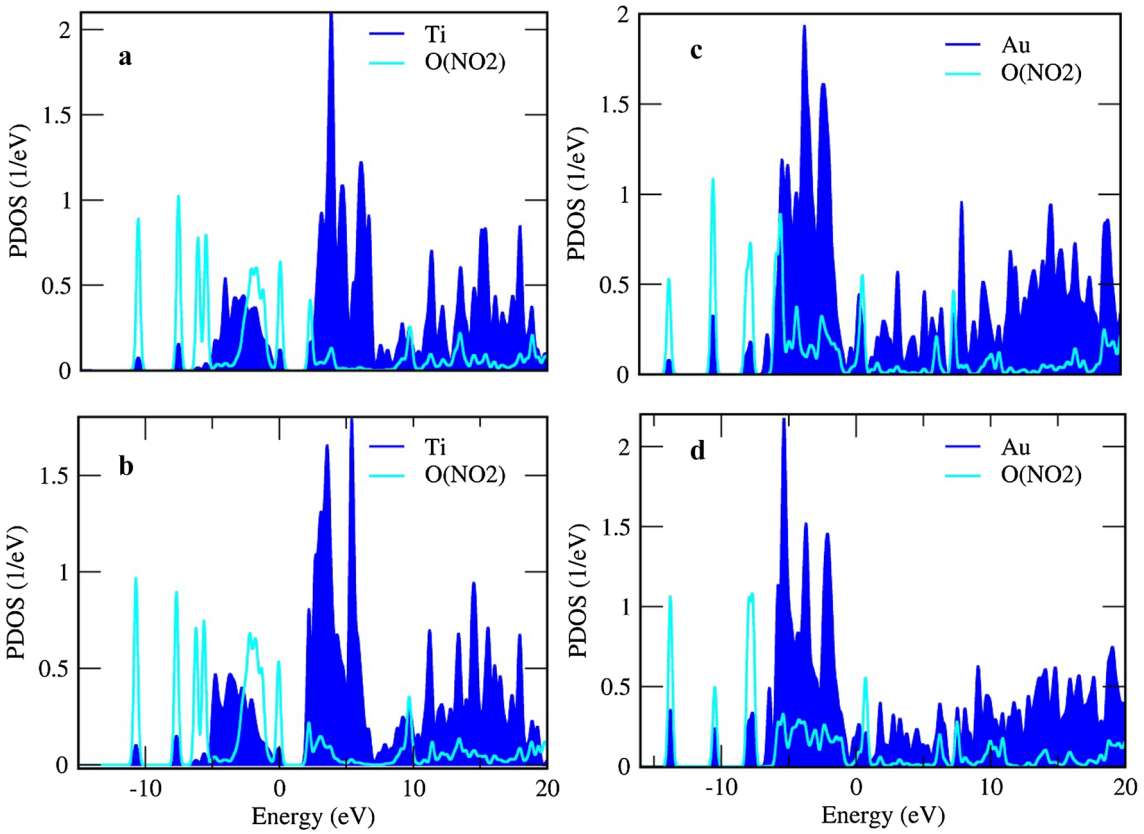

Fig. 7 PDOSs for the adsorption complexes of bare TiO_2 and Au nanoparticles with adsorbed NO_2 molecules. (**a**, **b**) Bare TiO_2–NO_2; (**c**, **d**) Bare Au–NO_2

summarizes the adsorption energies of NO_2 molecules adsorbed on the pristine TiO_2-supported Au nanoparticles. Of the three configurations, configuration A has the highest value of adsorption energy, thus making it the most favorable adsorption configuration and, consequently, the most likely binding site to be located on the TiO_2-supported Au.

Therefore, the adsorption of NO_2 on the TiO_2-supported Au nanoparticle (configuration A) is more favorable in energy than the adsorptions in configurations B and C. For both adsorption types A and C, the adsorption energy is higher (more negative) than the adsorption energy of adsorption type B. The reason is that the configurations A and C provide a double contacting point between the NO_2 and TiO_2-supported Au, whereas configuration B shows a single contacting point. NO_2 molecule was strongly coordinated to the TiO_2-supported Au by its two oxygen atoms. In other words, two oxygen atoms of the NO_2 molecule can interact with the TiO_2-supported Au overlayer more efficiently. The adsorption energies calculated from DFT-D2 and DFT-D3 methods are significantly larger than those obtained from the standard DFT calculations. Tamijani et al. [52] reported the results of the adsorption of noble-gas atoms on the TiO_2 (110) surface-based van der Waals corrected DFT approach and clearly demonstrated the increase in the adsorption energies caused by vdW interactions.

The adsorption energies are considerably increased when the adsorption energies are corrected for dispersion energy, as shown in Table 3. We have calculated the adsorption energies for NO_2 molecule on the bare Au and TiO_2 nanoparticles. As can be seen from Table 3, the adsorption energy of NO_2 molecule on the Au nanoparticle is about -1.23 eV and that of pristine TiO_2 is -0.72 eV, and NO_2 adsorption on the TiO_2-supported Au nanocomposite is found to be -1.48 eV. The higher adsorption energy gives rise to a strong interaction between the adsorbent and adsorbed molecules, and its more negative sign also represents an energy favorable process. Thus, NO_2 adsorption on the TiO_2-supported Au nanocomposite is more energetically favorable than the adsorption on the bare Au and TiO_2 nanoparticles. In the TiO_2-supported Au overlayers, the interactions of NO_2 and TiO_2 are stronger than those between NO_2 and bare TiO_2 nanoparticles, indicating that Au nanoparticle is conducive to the interaction of NO_2 molecule with TiO_2 nanoparticles. In other words, Au nanoparticle enhances NO_2 detection by means of the TiO_2-supported Au nanocomposite-based sensors.

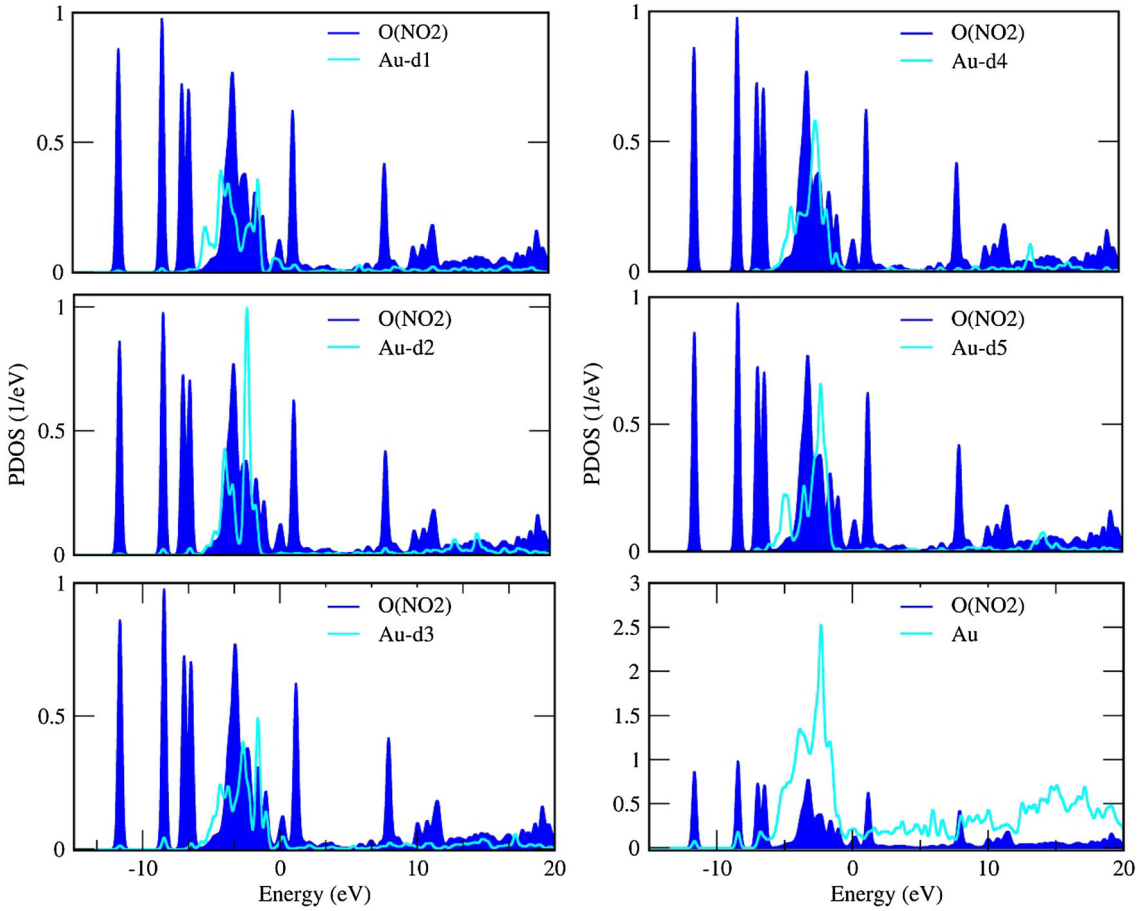

Fig. 8 PDOSs of the oxygen atom of NO_2 molecule and five *d* orbitals of the Au atom for the TiO_2-supported Au overlayers with adsorbed NO_2 molecules (configuration A)

Therefore, the results of adsorption energies suggest that the TiO_2-supported Au nanoparticle is a good candidate to be utilized in sensing of toxic NO_2 molecules in the environment.

Electronic structures

Figure 6 displays the projected density of states (PDOSs) for NO_2 adsorbed on the pristine TiO_2-supported Au overlayers. Panels (a, b) in this figure show the PDOSs of the Au atom of gold nanoparticle and oxygen atoms of the NO_2 molecule (configuration A). The great overlaps between the PDOSs of these two atoms indicate that the Au atoms form chemical bonds with the oxygen atoms of NO_2. In panels (c, d), we can see also the PDOSs of the Au atom of gold nanoparticle and the nitrogen atoms (configuration B), indicating substantial overlaps and thus formation of chemical Au–N bond. For configuration C, the pertinent PDOSs of the oxygen atoms of NO_2 molecule and the Au atoms are displayed in panels (e, f). As distinct from these PDOSs, the large overlaps show that both oxygen atoms of NO_2 molecule form chemical bonds with the Au atoms of the gold nanoparticle. This delivers a double interaction point between the NO_2 and TiO_2-supported Au. The interaction of NO_2 molecule with bare Au and TiO_2 nanoparticles was also examined, and the relevant PDOSs are shown in Fig. 7, representing noticeable overlaps between the PDOSs of the interacting atoms. This implies that the gold and titanium atoms form chemical bonds with the oxygen atoms of NO_2.

We also presented the PDOSs of five *d* orbitals of the Au atom and the oxygen atoms of the NO_2 molecule (configuration A). Figures 8, 9 show the PDOSs of the oxygen atom of NO_2 and different *d* orbitals of the Au atom, representing higher overlaps between the PDOSs of the oxygen with d^3 orbital of the Au atom. This indicates that the oxygen atom has a substantial mutual interaction with the d^3 orbital of the Au atom. Similarly, Fig. 10 displays the PDOSs of the nitrogen atom of the NO_2 and *d* orbitals of the Au atom, demonstrating noticeable overlaps between the nitrogen atom and d^2 orbital. For configuration C, the calculated PDOSs of the atom and different orbitals of Au atom are represented in Fig. S2.

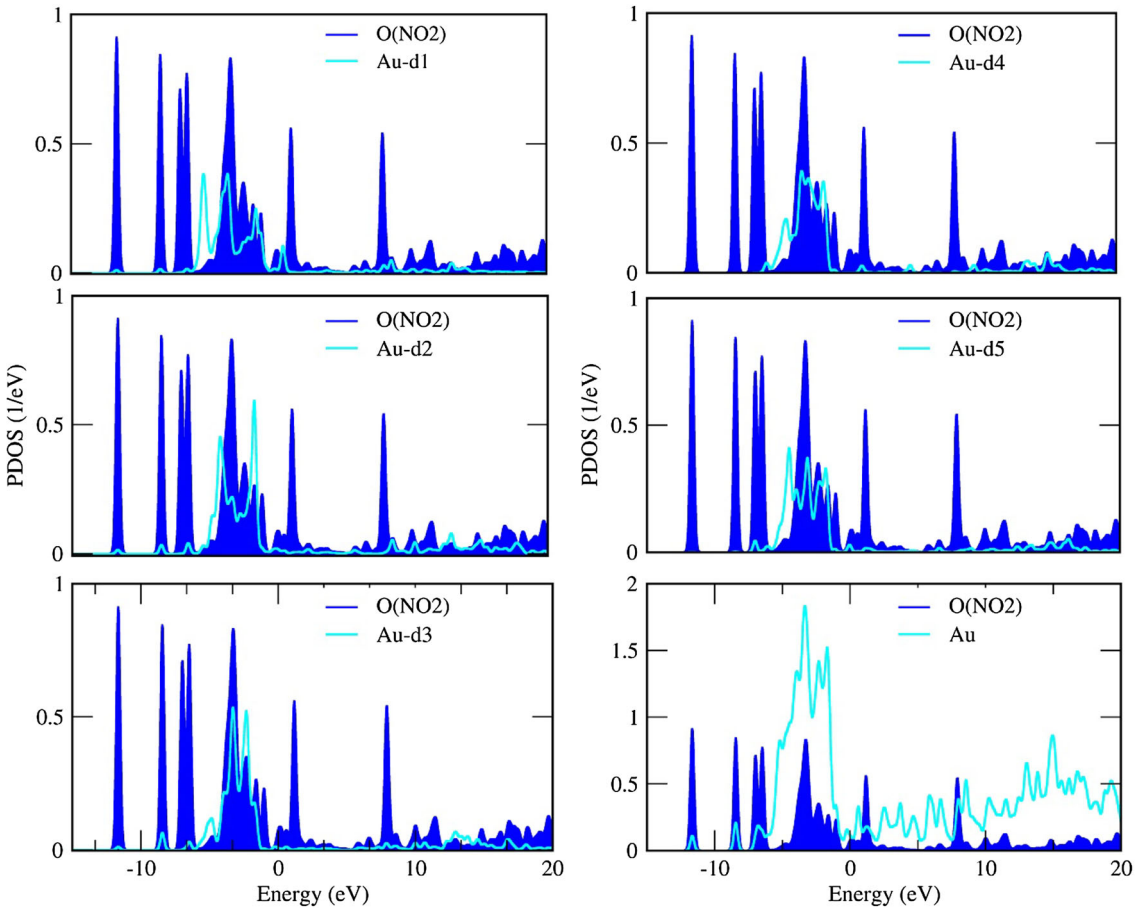

Fig. 9 PDOSs of the oxygen atom of NO_2 molecule and five *d* orbitals of the Au atom for the TiO_2-supported Au overlayers with adsorbed NO_2 molecules (configuration A)

We geometrically optimized the structure of TiO_2 anatase, and then calculated its band structure. The energy band structure of pristine anatase system is shown in Fig. 11. This figure represents that the calculated band structure of the valence band maximum (VBM) and the conduction band minimum (CBM) was both positioned at the G point. It also represents that pristine TiO_2 was a direct-gap semiconductor material. The calculated band-gap (BG) energy was 2.16 eV for TiO_2 anatase, which was slightly lower than the experimental result of 3.2 eV. Important to note is that, the electronic structure calculation using GGA pseudo-potential usually underestimates energy bandgaps [53, 54]. This band-gap underestimation is mostly ascribed to the well-known limitation of the exchange–correlation functional in describing excited states. Here, valance band corresponds to the O 2*p* orbitals and the conduction band arises from Ti 3*d* orbitals.

Mulliken charge analysis

The Mulliken population analysis was also conducted in this work to fully describe the charge exchange between the NO_2 molecule and TiO_2-supported Au overlayer. This method of charge analysis provides a means of estimating partial atomic charges from calculations implemented by computational chemistry packages. The calculated Mulliken charge values are listed in Table 3. This method assigns an electronic charge to a given atom in the considered system, that is, the gross atom population (GAP). The charge difference, ΔQ_A, is a measure of the difference between the number of electrons on the isolated free atom (Z_A) and the gross atom population:

$$\Delta Q_A = Z_A - \mathrm{GAP}_A. \quad (2)$$

For instance, configuration A represents a sizeable charge transfer of about 0.15 $|e|$ (e, the electron charge) from the TiO_2-supported Au nanoparticle to the NO_2 molecule, implying that NO_2 plays an important role as a charge acceptor. It is worth mentioning that the charge exchange between adsorbent and adsorbed molecule affects the conductivity of the system, being a great strategy to design more efficient and more appropriate sensor devices for the detection of NO_2 in the environment.

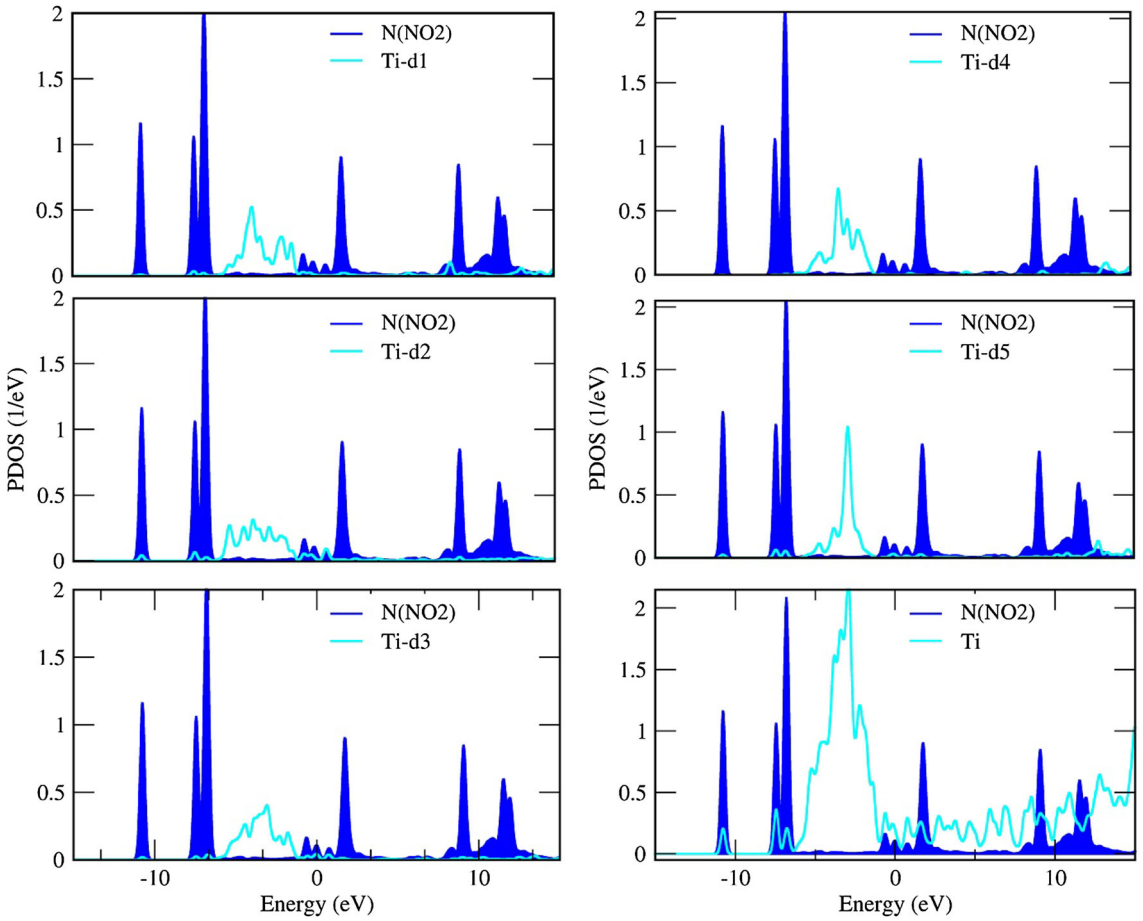

Fig. 10 PDOS of the nitrogen atom of NO_2 molecule and five *d* orbitals of the Au atom for the TiO_2-supported Au overlayers with adsorbed NO_2 molecules (configuration B)

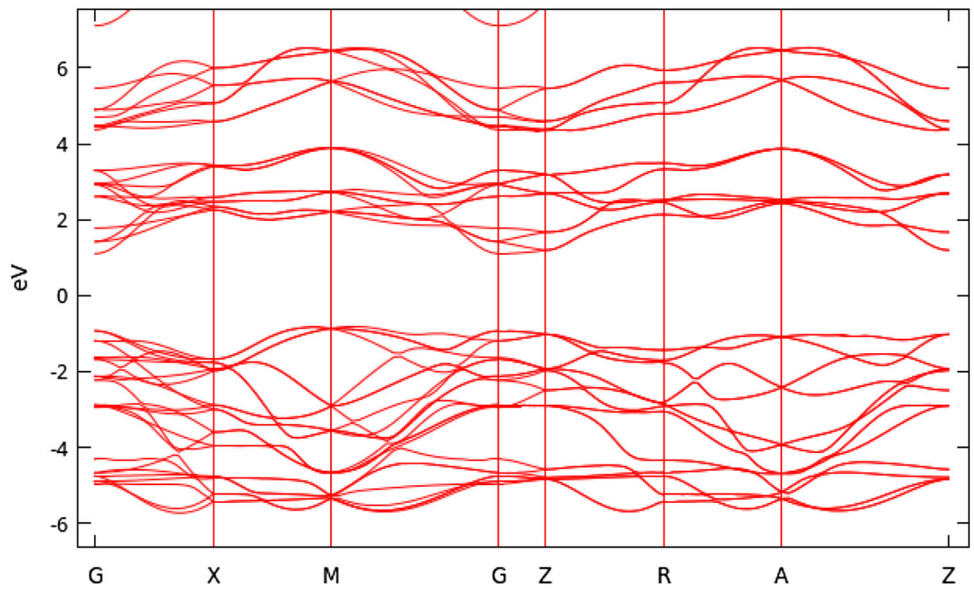

Fig. 11 Electronic band structure of pristine (undoped) TiO_2 anatase

One of the most important problems in Mulliken charge analysis is the intense sensitivity of Mulliken charges to the basis set choice. Fundamentally, a comprehensive basis set for a molecule can be covered by placing a large set of functions on a single atom. In the Mulliken scheme, all the electrons would then be assigned to the single atom. Therefore, it is well known that the Mulliken charge approach has no complete basis set limit, as the precise value which strongly depends on the way the limit is approached. Consequently, an efficient convergence for charges does not exist, and different basis set families may produce extremely different results. To overcome this problem, many modern approaches can be tried for estimating net atomic charges, such as electrostatic potential and natural population methods [55]. We have also calculated the Mulliken charges with the large basis sets of higher accuracy and then found that increasing basis set can simply modify Mulliken charges by approximately 0.22 *e*. The obtained results are summarized in Table 3. This table shows that the strong basis sets give rise to an increase in the Mulliken charge values.

Conclusions

DFT calculations were carried out to investigate the sensing performance of undoped TiO_2-supported Au nanoparticles for the detection of NO_2 molecules. The adsorption behaviors of NO_2 on the TiO_2-supported Au nanoparticles were investigated in detail. The results show that the N–O bonds of the adsorbed NO_2 molecule were elongated after the adsorption process, which indicates the weakening N–O bonds of the NO_2 molecule. The results also suggest that the interaction of the NO_2 molecule with the TiO_2-supported Au overlayer through its oxygen atoms is energetically more favorable than the interaction of NO_2 through its nitrogen atom. This interaction provides a double interacting point between the NO_2 and TiO_2-supported Au, suggesting the strong adsorption of NO_2 over the substrate. The current results suggest that Au nanoparticle in the TiO_2-supported Au nanocomposites affects the final configuration of TiO_2 nanoparticles with adsorbed NO_2 molecules and, therefore, strengthens the interaction between NO_2 and TiO_2. The substantial overlaps between the PDOSs of the Au and oxygen atoms, as well as, Au and nitrogen atoms indicate the formation of chemical bonds between them. Mulliken population analysis reveals a noticeable charge transfer from the TiO_2-supported Au to the NO_2 molecule, indicating the acceptor characteristic of the NO_2 molecule. Based on the inclusion of vdW interactions, we found that the adsorption energies become larger. However, our findings thus suggest that the TiO_2-supported Au nanoparticles can be utilized as potentially efficient gas sensors for NO_2 recognition.

Acknowledgements This work was supported by Azarbaijan Shahid Madani University.

References

1. Fujishima, A., Honda, K.: Electrochemical photolysis of water at a semiconductor electrode. Nature **238**, 37–38 (1972)
2. Fujishima, A., Hashimoto, K., Watanabe, T.: TiO_2 photocatalysis: fundamentals and applications. Bkc, Tokyo (1999)
3. Abbasi, A., Sardroodi, J.J.: N-doped TiO_2 anatase nanoparticles as a highly sensitive gas sensor for NO_2 detection: insights from DFT computations. J. Environ. Sci. Nano. **3**, 1153–1164 (2016)
4. Abbasi, A., Sardroodi, J.J.: Modified N-doped TiO_2 anatase nanoparticle as an ideal O_3 gas sensor: insights from density functional theory calculations. J. Comp. Theor. Chem. **600**, 2457–2469 (2016)
5. Fujishima, A., Zhang, X., Tryk, D.A.: TiO_2 photocatalysis and related surface phenomena. J. Surf. Sci. Rep. **63**, 515–582 (1992)
6. Batzilla, M., Morales, E.H., Diebold, U.: Surface studies of nitrogen implanted TiO_2. J. Chem. Phys. **339**, 36–43 (2007)
7. Isley, S.L., Penn, R.L.: Relative brookite and anatase content in sol–gel synthesized titanium dioxide nanoparticles. J. Phys. Chem. B **110**, 15134 (2006)
8. Rumaiz, A.K., Woicik, J.C., Cockayne, E., Lin, H.Y., Jaffari, G.H., Shah, S.I.: Oxygen vacancies in N doped anatase TiO_2: experiment and first-principles calculations. J. Appl. Phys. Lett. **95**, 262111 (2009)
9. Buonsanti, R., Grillo, V., Carlino, E., Giannini, C., Kipp, T., Cingolani, R., Cozzoli, P.D.: Nonhydrolytic synthesis of high-quality anisotropically shaped brookite TiO_2 nanocrystals. J. Am. Chem. Soc. **130**, 11223–11233 (2008)
10. Cassaignon, S., Koelsch, M., Jolivet, J.P.: Selective synthesis of brookite, anatase and rutile nanoparticles: thermolysis of $TiCl_4$ in aqueous nitric acid. J. Mater. Sci. **42**, 6689–6695 (2007)
11. Di Paola, A., Addamo, M., Bellardita, M., Cazzanelli, E., Palmisano, L.: Preparation of photocatalytic brookite thin films. Thin Solid Films **515**(7), 3527–3529 (2007)
12. Djaoued, Y., Bruning, R., Bersani, D., Lottici, P.P., Badilescu, S.: Sol–gel nanocrystalline brookite-rich titania films. Mater. Lett. **58**(21), 2618–2622 (2004)
13. Iskandar, F., Nandiyanto, A.B.D., Yun, K.M., Hogan, C.J., Okuyama, K., Biswas, P.: Enhanced photocatalytic performance of brookite TiO_2 macroporous particles prepared by spray drying with colloidal templatings. Adv. Mater. **19**, 1408–1412 (2007)
14. Kobayashi, M., Petrykin, V.V., Kakihana, M.: One-step synthesis of TiO2 (B) nanoparticles from a water-soluble titanium complex. Chem. Mater. **19**, 5373–5376 (2007)
15. Li, J.G., Ishigaki, T., Sun, X.D.: Anatase, brookite, and rutile nanocrystals via redox reactions under mild hydrothermal conditions: phase-selective synthesis and physicochemical properties. J. Phys. Chem. C **111**, 4969–4976 (2007)

16. Reddy, M.A., Kishore, M.S., Pralong, V., Caignaert, V., Varadaraju, U.V.: Room temperature synthesis and Li insertion into nanocrystalline rutile TiO_2. Electrochem. Commun. **8**(8), 1299–1303 (2006)
17. Shibata, Y., Irie, H., Ohmori, M., Nakajima, A., Watanabe, T., Hashimoto, K.: Comparison of photochemical properties of brookite and anatase TiO_2 films. Phys. Chem. Chem. Phys. **6**, 1359–1362 (2007)
18. Haruta, M., Kobayashi, T., Sano, H., Yamada, N.: Novel gold catalysts for the oxidation of carbon monoxide at a temperature far below 0 & #xB0;C. J. Chem. Lett. **16**(2), 405–408 (1987)
19. Landon, P., Collier, P.J., Papworth, A.J., Kiely, C.J., Hutchings, G.J.: Direct formation of hydrogen peroxide from H_2/O_2 using gold catalysts. Chem. Commun. **18**, 2058 (2002)
20. Molina, L.M., Hammer, B.: Some recent theoretical advances in the understanding of the catalytic activity of Au. Appl. Catal. A Gen. **291**, 21–31 (2005)
21. Okumura, M., Tsubota, S., Haruta, M.: Preparation of supported gold catalysts by gas-phase grafting of gold acethylacetonate for low-temperature oxidation of CO and of H_2. J. Mol. Catal. A: Chem. **199**, 73–84 (2003)
22. Lopez, N., Norskov, J.K.: Catalytic CO oxidation by a gold nanoparticle: a density functional study. J. Am. Chem. Soc. **124**, 11262–11263 (2002)
23. Chen, M.S., Goodman, D.W.: Structure–activity relationships in supported Au catalysts. Catal. Today. **111**, 22–33 (2006)
24. Kung, H.H., Kung, M.C., Costello, C.K.: Supported Au catalysts for low temperature CO oxidation. J. Catal. **216**, 425–432 (2003)
25. Hayashi, T.M., Tanaka, K., Haruta, M.: Selective vapor-phase epoxidation of propylene over Au/TiO_2 catalysts in the presence of oxygen and hydrogen. J. Catal. **178**, 566–575 (1998)
26. Salama, T., Ohnishi, R., Shido, T., Ichikawa, M.: Highly selective catalytic reduction of NO by H_2 over Au 0 and Au(I) impregnated in NaY zeolite catalysts. J. Catal. **162**(2), 169–178 (1996)
27. Rodriguez, J.A., Liu, G., Jirsak, T., Hrbek, J., Chang, Z.P., Dvorak, J., Maiti, A.: Activation of gold on titania: adsorption and reaction of SO_2 on Au/TiO2 (110). J. Am. Chem. Soc. **124**, 5242–5250 (2002)
28. Chen, M.S., Goodman, D.W.: The structure of catalytically active gold on titania. Science **306**(5694), 252–255 (2004)
29. Cosandey, F., Madey, T.E.: Growth, morphology, interfacial effects and catalytic properties of au on TiO_2. Surf. Rev. Lett. **8**, 73 (2001)
30. Vittadini, A., Selloni, A.: Small gold clusters on stoichiometric and defected TiO_2 anatase (101) and their interaction with CO: a density functional study. J. Chem. Phys. **117**, 353–361 (2002)
31. Chrétien, S., Metiu, H.: O_2 evolution on a clean partially reduced rutile TiO_2 (110) surface and on the same surface precovered with Au_1 and Au_2: the importance of spin conservation. J. Chem. Phys. **127**, 084704 (2007)
32. Molina, L.M., Rasmussen, M.D., Hammer, B.: Adsorption of O_2 and oxidation of CO at Au nanoparticles supported by TiO_2 (110). J. Chem. Phys. **120**(16), 7673 (2004)
33. Lin, C., Wen, G., Liang, A., Jiang, Z.: A new resonance Rayleigh scattering method for the determination of trace O_3 in air using rhodamine 6G as probe. J. RSC. Adv. **3**, 6627–6630 (2013)
34. Hohenberg, P.M., Kohn, W.: Inhomogeneous electron gas. J. Phys. Rev. **16**, B864–B868 (1964)
35. Kohn, W., Sham, L.: Self-consistent equations including exchange and correlation effects. J. Phys. Rev. **140**, A1133–A1138 (1965)
36. Ozaki, T., Kino, H., Yu, J., Han, M.J., Kobayashi, N., Ohfuti, M., Ishii, F., et al.: The code OpenMX, pseudoatomic basis functions, and pseudopotentials are available on a web site 'http://www.openmxsquare.org' (2017). Accessed 2 Mar 2017
37. Ozaki, T.: Variationally optimized atomic orbitals for large-scale electronic structures. J. Phys. Rev. B **67**, 155108 (2003)
38. Ozaki, T., Kino, H.: Numerical atomic basis orbitals from H to Kr. J. Phys. Rev. B **69**, 195113 (2004)
39. Perdew, J.P., Burke, K., Ernzerhof, M.: Generalized gradient approximation made simple. J. Phys. Rev. Lett. **78**, 1396 (1981)
40. Koklj, A.: Computer graphics and graphical user interfaces as tools in simulations of matter at the atomic scale. J. Comput. Mater. Sci. **28**, 155–168 (2003)
41. Grimme, S.: Semiempirical GGA-type density functional constructed with a long-range dispersion correction. J. Comput. Chem. **27**, 1787–1799 (2006)
42. Grimme, S., Antony, J., Ehrlich, S., Krieg, H.: A consistent and accurate ab initio parametrization of density functional dispersion correction (DFT-D) for the 94 elements H–Pu. J. Chem. Phys. **132**, 154104 (2010)
43. Grimme, S., Ehrlich, S., Goerigk, L.: Effect of the damping function in dispersion corrected density functional theory. J. Comput. Chem. **32**, 1456–1465 (2011)
44. Downs, R.T.: Web page at: http://rruff.geo.arizona.edu/AMS/amcsd.php (2014). Accessed 9 May 2014
45. Wyckoff, R.W.G.: Crystal structures, 2nd edn. Interscience Publishers, New York (1963)
46. Lei, Y., Liu, H., Xiao, W.: First principles study of the size effect of TiO_2 anatase nanoparticles in dye-sensitized solar cell. Modelling Simul. Mater. Sci. Eng. **18**, 025004 (2010)
47. Liu, J., Dong, L., Guo, W., Liang, T., Lai, W.: CO adsorption and oxidation on N-doped TiO_2 nanoparticles. J. Phys. Chem. C **117**, 13037–13044 (2013)
48. Lazzeri, M., Vittadini, A., Selloni, A.: Structure and energetics of stoichiometric TiO_2 anatase surfaces. Phys. Rev. B. **63**, 155409 (2001)
49. Wu, C., Chen, M., Skelton, A.A., Cummings, P.T., Zheng, T.: Adsorption of arginine–glycine–aspartate tripeptide onto negatively charged rutile (110) mediated by cations: the effect of surface hydroxylation. ACS Appl. Mat. Interfaces **5**, 2567–2579 (2013)
50. Liu, J., Liu, Q., Fang, P., Pan, C., Xiao, W.: First principles study of the adsorption of a NO molecule on N-doped anatase nanoparticles. J. Appl. Surf. Sci. **258**, 8312–8318 (2012)
51. Breedon, M., Spence, R.M., Yarovsky, I.: Adsorption of NO_2 on oxygen deficient ZnO (2110) for gas Sensing applications: a DFT study. J. Phys. Chem. C **14**(39), 16603–16610 (2010)
52. Tamijani, A.A., Salam, A., de-Lara-Castells, P.: Adsorption of noble-gas atoms on the TiO2 (110) surface: an ab initio assisted study with van der Waals corrected DFT. J. Phys. Chem. C **120**(32), 18126–18139 (2016)
53. Longa, M., Cai, W., Wang, Z., Liu, G.: Correlation of electronic structures and crystal structures with photocatalytic properties of undoped, N-doped and I-doped, TiO_2. Chem. Phys. Lett. **420**, 71–76 (2006)
54. Gao, H., Zhou, J., Dai, D., Qu, Y.: Photocatalytic activity and electronic structure analysis of N-doped anatase TiO_2: a combined experimental and theoretical study. Chem. Eng. Technol. **32**(9), 867–872 (2009)
55. Reed, A.E., Weinstock, R.B., Weinhold, F.: Natural population analysis. J. Chem. Phys. **83**(2), 735–746 (1985)